LETTERS

Coordination of Rho GTPase activities during cell protrusion

Matthias Machacek[1]*†, Louis Hodgson[2]*†, Christopher Welch[2]*, Hunter Elliott[1], Olivier Pertz[1]†, Perihan Nalbant[3], Amy Abell[2], Gary L. Johnson[2], Klaus M. Hahn[2] & Gaudenz Danuser[1]

The GTPases Rac1, RhoA and Cdc42 act together to control cytoskeleton dynamics[1–3]. Recent biosensor studies have shown that all three GTPases are activated at the front of migrating cells[4–7], and biochemical evidence suggests that they may regulate one another: Cdc42 can activate Rac1 (ref. 8), and Rac1 and RhoA are mutually inhibitory[9–12]. However, their spatiotemporal coordination, at the seconds and single-micrometre dimensions typical of individual protrusion events, remains unknown. Here we examine GTPase coordination in mouse embryonic fibroblasts both through simultaneous visualization of two GTPase biosensors and using a 'computational multiplexing' approach capable of defining the relationships between multiple protein activities visualized in separate experiments. We found that RhoA is activated at the cell edge synchronous with edge advancement, whereas Cdc42 and Rac1 are activated 2 μm behind the edge with a delay of 40 s. This indicates that Rac1 and RhoA operate antagonistically through spatial separation and precise timing, and that RhoA has a role in the initial events of protrusion, whereas Rac1 and Cdc42 activate pathways implicated in reinforcement and stabilization of newly expanded protrusions.

Our computational multiplexing approach makes the assumption that the relationship between GTPase activation and the movements of the cell edge during constitutive protrusion and retraction cycles is preserved within a cell, and among cells. Thus, the initiation of protrusion and retraction can be used as a timing reference to determine indirectly the activation dynamics of multiple Rho GTPases: first, for each GTPase, the timing of activation relative to protrusion/retraction events is determined in separate experiments. Then, the activation timings of different GTPases are aligned, using protrusion/retraction events as a common reference. GTPase activities were imaged in mouse embryonic fibroblasts (MEFs) using biosensors for Rac1 (ref. 4), Cdc42 (ref. 5) or RhoA[6] (Fig. 1a–c and Supplementary Figs 1 and 2). The Rac1 biosensor was improved compared with the previously published version[4], using a fluorescent protein rather than a covalently attached dye. Images were captured at 10-s intervals, sufficient to sample the protrusion–retraction cycles below Nyquist frequency (Supplementary Fig. 3).

As reported before[4–6], all GTPases, including RhoA, were maximally activated proximal to the leading edge. Visual inspection of time-lapse sequences indicated substantial fluctuations in GTPase activity as the cell edges protruded and retracted (Supplementary Movies 1–6). To quantify the magnitude and location of the fluctuations we extracted time courses of GTPase activity at multiple distances from the cell edge and quantified the extent of signal modulation (Fig. 1d). For all three GTPases the modulation was highest at the cell edge, decreased monotonically within ~2–4 μm, and then reached a plateau of baseline activity (Fig. 1e–g). Rac1 displayed the least significant decay, mainly because of cell-to-cell variations in the extent of the region with high activation. RhoA, on the other hand, decayed tightly over 2 μm. Thus, GTPase activities are regulated most prominently within a few micrometres from the leading edge, supporting the hypothesis that these fluctuations may be linked to cell edge movements.

To investigate how GTPase activation relates to edge movement spatially and temporally, we tracked the position of the cell edge[13] and compared edge velocities with the biosensor signal in 40 to 80 sampling windows moving with the leading edge (Fig. 1h and Supplementary Movie 7). The window width was set to 1.8–3 μm, the distance over which edge movements were correlated along the cell boundary, and 0.9 μm in depth, the distance over which signalling molecules bound to the plasma membrane would be expected to diffuse between consecutive movie frames[14]. Edge velocities were sampled every 400 nm (see Methods), so that 5–7 velocity measurements would fall within a window (Fig. 1i). Thus, each window yielded time courses of both edge velocity and GTPase activation level (Fig. 1j), with independent measurements in each adjacent window. Changes in edge velocity appeared to parallel changes in GTPase activity (shown for the example of a Cdc42 data set), but with a time lag.

To study more systematically the potential relationships between edge dynamics (Fig. 2a, d, g) and GTPase activation we copied the data from the individual sampling windows along the cell boundary into activity maps[13] (Fig. 2b, c, e, f, h, i). This data representation revealed tight correlation of morphological dynamics and GTPase activation. Protrusion and retraction occurred in a quasi-cyclic fashion with a periodicity of ~100 s (Supplementary Fig. 3). As reported previously[13], protrusion cycles propagated transversally along the leading cell edge (Fig. 2b, e, h). Both Cdc42 and RhoA cycled with similar periodicity (Supplementary Fig. 3) and their activity maps visually resembled those of the morphological dynamics (Fig. 2f, i). Rac1 showed a broader time response (Supplementary Fig. 3), consistent with a spatiotemporally more diffuse activation (Fig. 2c). Quiescent regions of the cell edge (that is, regions Q) exhibited low GTPase activity compared with protruding and retracting regions. Transitions between active and quiescent portions of the cell edge were sharp (2–3 μm) and were accompanied by a steep gradient in GTPase activity. Thus, these data suggest an immediate coupling of GTPase activation and cell morphological dynamics, in both time and space.

To quantify the coupling we computed, for every sampling window, Pearson's correlation coefficient between edge velocity

[1]Department of Cell Biology, The Scripps Research Institute, 10550 N. Torrey Pines Road, La Jolla, California 92037, USA. [2]Departments of Pharmacology, Medicinal Chemistry and Lineberger Cancer Center, University of North Carolina at Chapel Hill, Chapel Hill, North Carolina 27599, USA. [3]Department of Molecular Cell Biology, Center for Medical Biotechnology, University of Duisburg-Essen, 45117 Essen, Germany. †Present addresses: Novartis Pharma AG, Lichtstrasse 35, CH-4056 Basel, Switzerland (M.M.); Department of Anatomy and Structural Biology and Gruss-Lipper Biophotonics Center, Albert Einstein College of Medicine of Yeshiva University, 1300 Morris Park Ave, Bronx, New York 10461, USA (L.H.); Department of Biomedicine, University of Basel, Mattenstrasse 28, CH-4058 Basel, Switzerland (O.P.).
*These authors contributed equally to this work.

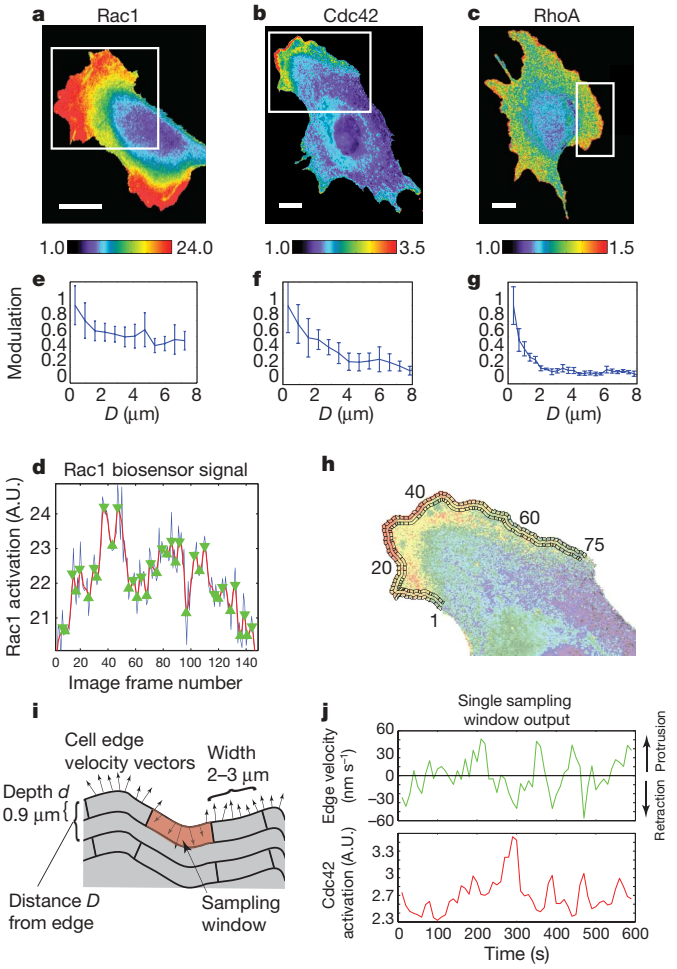

Figure 1 | Activation of Rho GTPases in migrating MEFs. **a**–**c**, Rac1 (**a**), Cdc42 (**b**) and RhoA (**c**) activation reported by biosensors. White box indicates region of interest selected for analysis. Scale bar, 20 μm. Colour scale indicates the dynamic range of the biosensor response (1, no significant response; maximum value, strongest response throughout the time-lapse sequence). **d**, Time course (blue line) of Rac1 activation within 0.6 μm from the cell edge, averaged over a 5-μm-long portion of the cell edge. Red line indicates filtered time course (Gaussian filter, $\sigma = 5$ frames). Green triangles indicate local maxima and minima of filtered time course. **e**–**g**, Modulation of GTPase activation (mean absolute difference between consecutive local extrema of the time course) as a function of the distance D from the leading edge. Values are normalized to the modulation at the cell edge. Error bars indicate s.e.m. of $n = 6$ (Rac1), $n = 4$ (Cdc42) and $n = 4$ (RhoA) cells. **h**, Sampling windows of 0.9-μm depth placed at the cell edge and at $D = 1.8$ μm from the cell edge. **i**, Parameters to define the position and size of a sampling window. In each window, the time course of GTPase activation was recorded (average of ~10 pixels). For a sampling window at $D = 0$, a time course of edge velocity was recorded (mean of 6–8 measurements). **j**, Time courses of edge velocity (green) and GTPase activation (Cdc42, red) recorded in one sampling window.

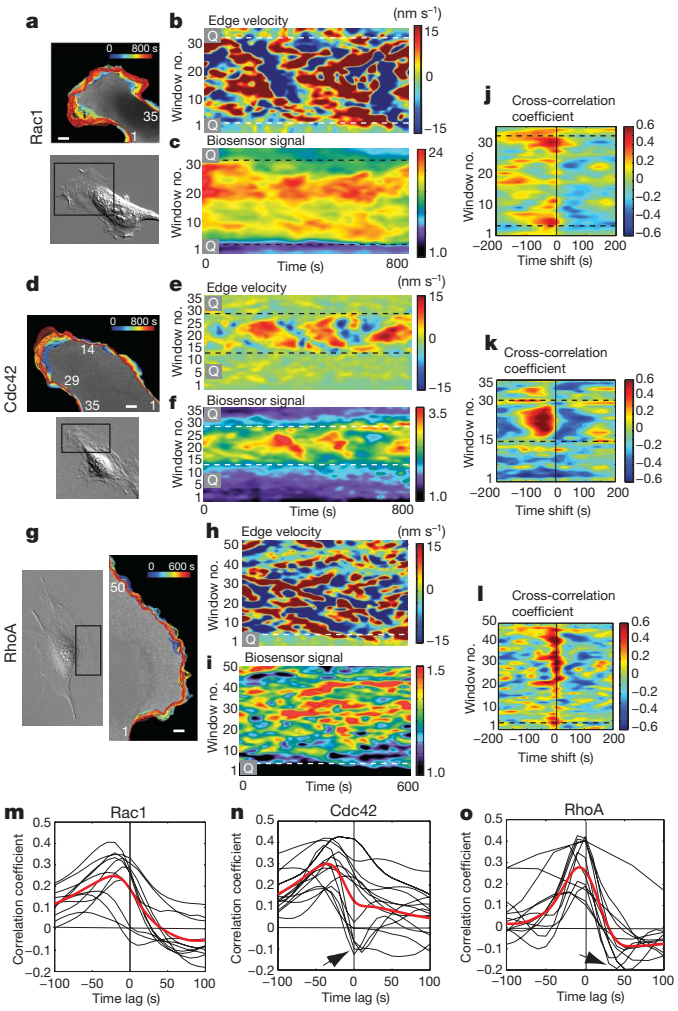

Figure 2 | Dynamics of cell edge morphology and GTPase activation. **a**, **d**, **g**, Overview of cell morphology (in DIC) and evolution of cell edge positions (colour-encoded from blue (early) to red (late) time points). Scale bar, 5 μm. **b**, **e**, **h**, Activity maps of edge movement: velocity values along the edge are copied time point by time point into the columns of the map. Colour coding: red, protrusion; blue, retraction. Quiescent regions of the cell edge are marked by 'Q'. **c**, **f**, **i**, Activity maps of Rho GTPase activation: colours designate the activation level of the Rho GTPase recorded in a sampling window at $D = 0$ μm. **j**, **k**, **l**, Cross-correlation coefficients (colour-coded) between edge velocity and Rac1 (**j**), Cdc42 (**k**) and RhoA (**l**) as a function of the sampling window and time shift. **m**, **n**, **o**, Temporal cross-correlation functions for individual cells (black). Red lines indicate average cross-correlation functions per GTPase resulting from a spline fit to the combined single-cell cross-correlation functions; $n = 11$ (Rac1), $n = 12$ (Cdc42) and $n = 12$ cells (RhoA). Some cells show negative correlation coefficients at positive time lags (arrowheads), probably associated with ruffling (see text).

and the GTPase activity, as a function of the time lag between the two variables. High correlation coefficients indicated a tight coupling of GTPase activation and cell protrusion/retraction events, whereas low correlation coefficients suggested a more remote relationship. Moreover, if a significant maximum correlation coefficient was obtained at a non-zero time lag, it indicated the relative timing of the two processes. For actively protruding regions, we observed significant correlation coefficients for all three GTPases. For Cdc42 and Rac1, high correlation values occurred predominantly at negative time lags (Fig. 2j, k), that is, the activation of these two GTPases was delayed relative to cell edge advancements. In contrast, for RhoA high correlation values were narrowly distributed around zero time lags (Fig. 2l). Thus, RhoA activation seemed to be synchronous with forward movements of the cell edge. These results show that GTPases are activated over a fixed time interval relative to the dynamics of the leading edge.

To estimate more precisely the activation of the three GTPases relative to protrusion/retraction events, we averaged the correlation coefficients over all sampling windows of a cell (Supplementary Fig. 4). A comparison between cells showed that despite substantial variation in shape and morphodynamic behaviour, the relationships between GTPase activation and edge movements were preserved (Fig. 2m–o). To estimate the average timing between protrusion/retraction and GTPase activation across cells the correlation coefficients of individual cells were pooled and the significant maximum of a spline function fitted through the data determined (Fig. 2m–o, red curves; Supplementary Methods). A few cells displayed correlation minima

at positive time lags, particularly with Cdc42 and RhoA (Fig. 2n, o, arrowheads). These were probably due to ruffling events in which GTPases reach a high activation level a few seconds before the lamellipodium is lifted off the substrate and the edge retracts (see Supplementary Movies 3–4). Edge retraction generates a negative velocity in the velocity map, and hence a negative cross-correlation with elevated GTPase activation. These ruffling events did not affect our finding that both Rac1 and Cdc42 activation lag edge protrusion, whereas RhoA is activated during cell protrusion.

We speculated that the GTPases might be organized not only temporally, but also spatially, within the band of modulated signalling activity (see Fig. 1e–g). Therefore, we repeated the correlation analysis between protrusion and retraction events and activation of Rac1, Cdc42 and RhoA in sampling windows at various distances from the cell edge (Fig. 3a–c, see also Supplementary Movie 7). Maxima of the correlation coefficients CM and the corresponding time lags Δt were determined for each distance and fitted with a smoothing spline (Fig. 3d–f). For RhoA the correlation coefficient was highest at the leading edge and monotonically decreased at larger distances from the edge (Fig. 3f, blue line). At $D > 2$ μm the correlation coefficient was smaller than 0.2 (Fig. 3d–f, black dashed line), the 95% confidence level for correlation coefficients of individual cells (Supplementary Methods). Thus, beyond 2 μm RhoA activity is no longer related to protrusion events (Fig. 3f, arrow). Rac1 and Cdc42 activities were correlated with edge movements over a wider region (4.5 μm and 3.2 μm, respectively; Fig. 3d, e, blue curve). Interestingly, the highest correlation coefficients were found at a distance $D = 1.8 \pm 0.7$ μm for Rac1 and at $D = 1.3 \pm 0.7$ μm for Cdc42. The same distance D was obtained when identifying the distance with the shortest time lag between edge velocity fluctuations and GTPase activation (Fig. 3d, e, red curve), which indicates the location of initial GTPase activation. These results indicate that both Rac1 and Cdc42 are activated at ~1.8 μm from the cell edge. The larger time lags and lower correlation coefficients at distances other than 1.8 μm suggest that the activation of Rac1 and Cdc42 then propagates in anterior and posterior directions, loosing the close coordination with edge movements.

Next, we estimated the between-cell variation of the cross-correlation time lag (Fig. 4a) by bootstrapping 2,000 samples from the residual distribution of the spline fit to the individual correlation functions in Fig. 2m–o. The time lags were consistently negative for all three GTPases, that is, the peak in their activation was delayed relative to the protrusion of the cell edge (time lag (s) to protrusion for Rac1, −41 (−61 −13); Cdc42, −46 (−51 −39); RhoA, −6 (−8 −4); mean ± 95% confidence interval as determined by bootstrap analysis). Hence, Rac1, Cdc42 and RhoA each have a different timing of activation, which is conserved between cells.

We were concerned that the measured spatiotemporal shifts of Rac1, Cdc42 and RhoA activation might be attributed to the different biosensor designs we used for each of these proteins (Supplementary Fig. 1). Some designs might be more susceptible to competition from native ligands, affecting readouts of activation kinetics. Therefore, we titrated the concentrations of biosensor components (Supplementary Figs 8 and 9) and repeated the timing experiments using different biosensor designs for the same GTPase (Supplementary Fig. 10). These control experiments confirmed that neither the relative activation kinetics nor the localization were a function of biosensor design (see Supplementary Materials).

We also sought to validate the time shifts between GTPase activations predicted by computational multiplexing by directly observing two signalling activities in the same cell. To this end, we modified the Cdc42 biosensor with new fluorophores (Supplementary Fig. 6), enabling simultaneous imaging of Cdc42 and RhoA activation in one cell (Movie 9). The resulting four-channel image data provided unprecedented temporal and spatial resolution for the study of the coordination between two signalling molecules, without using the cell edge velocity as a reference. Here, fluctuation correlation analysis was valuable to harness the full information from multiplex biosensor imaging. The data were again analysed locally in sampling windows at the leading edge. Averaging the correlation coefficients between the Cdc42 and RhoA time courses within one cell and over $n = 7$ cells we obtained a time lag of −34 (−30, −38) s, that is, Cdc42 was activated after RhoA (Fig. 4b). This was within the confidence band of the computationally predicted difference between Cdc42 and RhoA activation (see Fig. 4a), confirming that direct visualization and indirect inference of signalling relationships yield the same result.

Together, these data indicate the following dynamics of Rho family GTPase activation in one protrusion–retraction cycle (Fig. 4c): RhoA activation increases and decreases in synchrony with protrusion and retraction. RhoA activation that is correlated with leading edge dynamics is confined to a band 2 μm from the leading edge. Cdc42 and Rac1 reach their peak activation with a 40-s delay relative to protrusion, and their activation is initiated 1.8 μm from the leading edge. Rac1 and Cdc42 are temporally as well as spatially less coupled

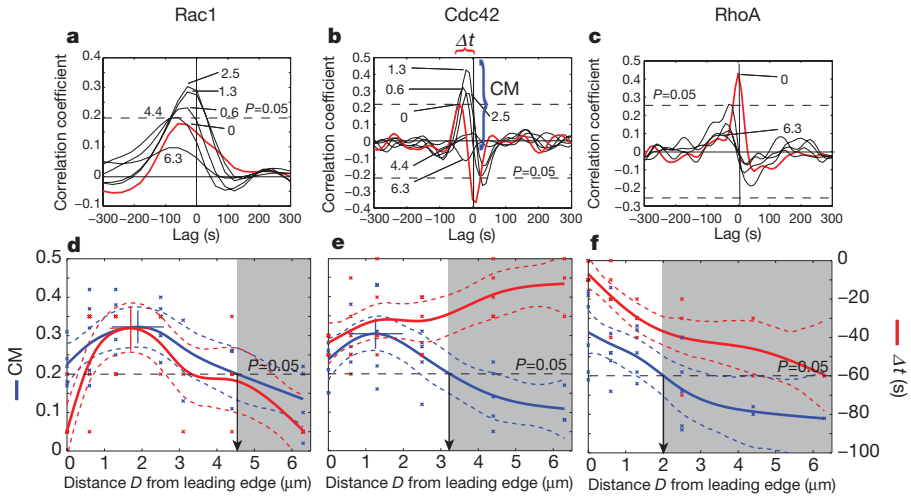

Figure 3 | Correlation of Rho GTPase activation and cell edge velocity as a function of time and space. a–c, Cross-correlation functions between edge velocity and GTPase activation at $D = 0$ (red line), 0.6, 1.3, 2.5, 4.4 and 6.3 μm. Dashed line indicates 95% confidence level for correlation values. **d–f**, Blue line indicates magnitude of cross-correlation maximum (CM has no units) as a function of D (blue bracket in **b**). Red line indicates time lag of cross-correlation maxima as a function of D (red bracket in **b**). Dashed lines indicate 95% confidence interval estimated by bootstrap sampling of residual distributions to the spline fits (see Supplementary Methods). Grey area indicates region with correlation values below 95% confidence. Of note, time lags of cross-correlation maxima in this area are no longer meaningful. Data derived from $n = 6$ (Rac1), $n = 5$ (Cdc42) and $n = 5$ (RhoA) cells.

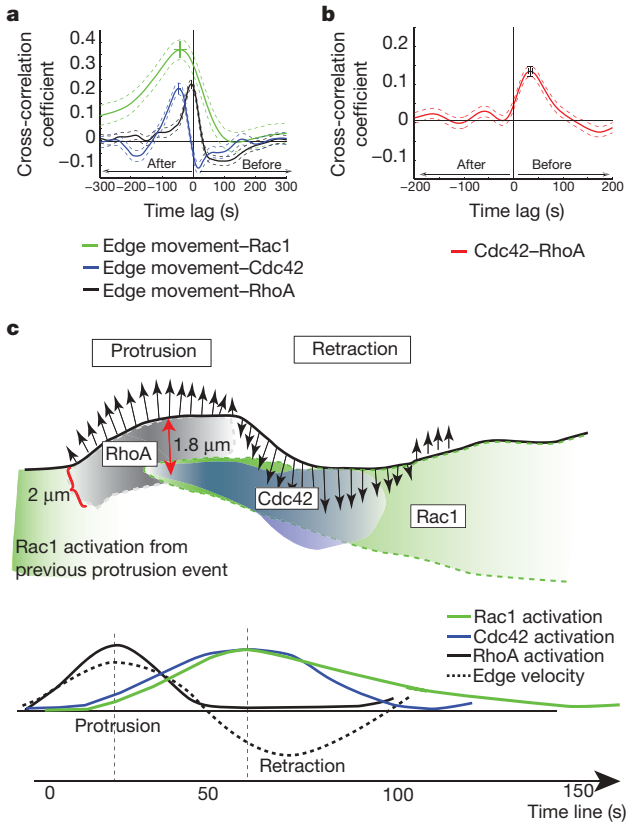

Figure 4 | Spatiotemporal coordination of Rac1, Cdc42 and RhoA activation. **a**, Timing of Rho GTPase activation relative to edge velocity, as determined by temporal cross-correlation functions. The variable 'edge movement' is being used as the reference signal. Thus, correlation maxima in the sector labelled 'After' indicate that the GTPase reaches the activation maximum after the protrusion event (time point of fastest edge advancement). Dashed lines indicate 95% confidence intervals. Data originate from $n = 11$ (Rac1), $n = 12$ (Cdc42) and $n = 12$ cells (RhoA). Confidence intervals were computed by bootstrap sampling of 2,000 residuals to the spline fits. **b**, Timing of RhoA activity relative to Cdc42 activity, both monitored in the same cell, as determined by the temporal cross-correlation function. The variable Cdc42 is being used as the reference signal. Thus, the correlation maximum in the sector labelled 'Before' indicates that RhoA reaches the activation maximum before Cdc42 ($n = 7$ cells). The y axes for panels **a** and **b** are without units. **c**, Model of GTPase activation during protrusion and retraction. Green indicates Rac1 activation; black, RhoA activation; blue, Cdc42 activation.

to protrusion. Cdc42, and even more so Rac1, maintain significant levels of activity during the retraction phase, such that lower levels of Rac1 activation overlap the onset of the next protrusion cycle. Rac1 and Cdc42 signals propagate from their location of initial activation in anterograde and retrograde directions via as-yet-unidentified mechanisms.

The delayed activation of Rac1 and Cdc42 suggests that in spontaneous cell motility, that is, without active stimulation by growth factors, their primary role may not be in initiating protrusion, as is currently supposed[15]. Although the early, low activation level of Rac1 we observe may still be sufficient for this role, the peak activities for Rac1 and Cdc42 are localized closer to the sites of maturating adhesions (~1.8 µm behind the protruding leading edge[16]). Rac1 and Cdc42 seem to be affecting protrusion by regulating adhesion dynamics[17–19], probably by reinforcing adhesion sites that are formed to balance increasing protrusive forces at the leading edge[20,21]. In addition, our data support the notion that Rac1 operates as an antagonist to RhoA[12]. RhoA activity is rapidly suppressed as Rac1 reaches its maximum activation. RhoA is usually thought to be a mediator of contractility. Here, we propose that the synchronized activation of RhoA with protrusion relates to a second function of RhoA as an initiator of actin polymerization at the onset of the protrusion–retraction cycle, possibly via its ability to activate members of the formin family such as mDia[22,23]. In addition, the RhoA–mDia pathway is known to stabilize microtubules specifically in leading edge adhesions[24]. This may contribute to the activation of Rac1 we observed at adhesion sites, perhaps via positive feedback between microtubule growth and Rac1 activation[25] and/or via the engagement of integrins that regulate the coupling of Rac1 to its effector Pak1[26], which is known to exhibit mutually positive feedback[18].

We present two complementary approaches to *in situ* analysis of cellular pathways. Simultaneous imaging presents unprecedented spatial and temporal resolution to explore the relationship between two pathways, whereas 'computational multiplexing' enables correlation of many signalling activities. Computational multiplexing makes use of the spontaneous activation of pathways by random local changes in signalling molecules due to low level stochastic stimulation of receptors, variations in concentration, and so on. Thus, it is potentially less perturbing than methods that rely on acute cell stimulation to initiate a signalling cascade. The sensitivity required to capture the coupling of spontaneous molecular activities is achieved for two reasons: first, by very local image measurement, below the diffusion radius of signalling molecules, our analysis captures the immediate relationship between the states of a signalling pathway and its morphological outputs. Although the activity levels of pathway components and hence the pathway outputs may vary between cellular locations and between cells, the hierarchy and timing between pathway components are conserved. Second, measurement noise is greatly reduced by averaging thousands of local relationships between activities. Together, these properties permit the pathway to be reconstructed despite significant cell-to-cell heterogeneity.

We chose to illustrate computational multiplexing for a pathway controlling cell morphology, enabling us to use cell morphological dynamics as a reference to align distinct signalling events observed in different experiments. However, the method is readily scalable to more and diverse activities. Relationships between signals can also be inferred in pathways without spatial cues. In this case, one of the biosensors may itself be used as the common reference in a series of experiments where it is imaged simultaneously in pairings with other biosensors. Again, the statistical approaches described for computational multiplexing will be useful to integrate into a pathway model the heterogeneous and complex responses made visible by simultaneous imaging of different biosensor combinations.

METHODS SUMMARY

Biosensors. The three biosensors were made and used as originally described[4–6], with modifications where noted in the text. The Cdc42 biosensor was modified for multiplex imaging by removing EGFP and replacing it with an Alexa750 dye. This produced a biosensor with wavelengths orthogonal to those of the RhoA biosensor. The new Cdc42 biosensor was fused to maltose-binding protein to enhance solubility. For control studies a new dual-chain RhoA biosensor was constructed by eliminating the linker in the published RhoA biosensor (see Supplementary Information).

Live cell imaging. Biosensors were imaged as previously described[27,28]. In order to obtain sufficient signal/noise for multiplexing, cells with biosensor were filmed at 10-s intervals, using a 40×/1.3 NA objective and binning, resulting in an effective pixel size in object space of 330 nm.

Ratiometric corrections. Raw images were aligned and noise-filtered to allow ratiometric correction of volume effects, bleed-through and variation in sensor concentration.

Image analysis. Corrected biosensor images were segmented and cell edge displacements tracked as in ref. 13. Sampling windows of 0.9 µm depth and 1.8–3 µm width were constructed to follow morphological changes at a fixed distance from the cell edge. For each window, biosensor activation time courses were recorded. For windows placed at the cell edge, a time course of protrusion/retraction velocity was recorded additionally. Coupling of two activity time courses was analysed per window by Pearson's cross-correlation function. Subsequently, for a cell the per-window correlation functions were averaged over all windows following the edge at a specific distance D (Fig. 1i). Per-cell correlation functions were averaged over multiple cells and statistically analysed

by bootstrap sampling to determine the significance and time lag of the coupling between two activities. All procedures are detailed in Supplementary Methods.

Received 5 January; accepted 24 June 2009.
Published online 19 August; corrected 3 September 2009 (see full-text HTML version for details).

1. Jaffe, A. B. & Hall, A. Rho GTPases: biochemistry and biology. *Annu. Rev. Cell Dev. Biol.* **21,** 247–269 (2005).
2. Burridge, K. & Wennerberg, K. Rho and Rac take center stage. *Cell* **116,** 167–179 (2004).
3. Ridley, A. J. *et al.* Cell migration: integrating signals from front to back. *Science* **302,** 1704–1709 (2003).
4. Kraynov, V. *et al.* Localized Rac activation dynamics visualized in living cells. *Science* **290,** 333–337 (2000).
5. Nalbant, P., Hodgson, L., Kraynov, V., Toutchkine, A. & Hahn, K. M. Activation of endogenous Cdc42 visualized in living cells. *Science* **305,** 1615–1619 (2004).
6. Pertz, O., Hodgson, L., Klemke, R. L. & Hahn, K. M. Spatiotemporal dynamics of RhoA activity in migrating cells. *Nature* **440,** 1069–1072 (2006).
7. Kurokawa, K. & Matsuda, M. Localized RhoA activation as a requirement for the induction of membrane ruffling. *Mol. Biol. Cell* **16,** 4294–4303 (2005).
8. Nobes, C. D. & Hall, A. Rho, rac, and cdc42 GTPases regulate the assembly of multimolecular focal complexes associated with actin stress fibers, lamellipodia, and filopodia. *Cell* **81,** 53–62 (1995).
9. Rottner, K., Hall, A. & Small, J. V. Interplay between Rac and Rho in the control of substrate contact dynamics. *Curr. Biol.* **9,** 640–649 (1999).
10. Nimnual, A. S., Taylor, L. J. & Bar-Sagi, D. Redox-dependent downregulation of Rho by Rac. *Nature Cell Biol.* **5,** 236–241 (2003).
11. Arthur, W. T., Burridge, K. & Rho, A. Inactivation by p190RhoGAP regulates cell spreading and migration by promoting membrane protrusion and polarity. *Mol. Biol. Cell* **12,** 2711–2720 (2001).
12. Ohta, Y., Hartwig, J. H. & Stossel, T. P. FilGAP, a Rho- and ROCK-regulated GAP for Rac binds filamin A to control actin remodelling. *Nature Cell Biol.* **8,** 803–814 (2006).
13. Machacek, M. & Danuser, G. Morphodynamic profiling of protrusion phenotypes. *Biophys. J.* **90,** 1439–1452 (2006).
14. Marguet, D., Lenne, P. F., Rigneault, H. & He, H. T. Dynamics in the plasma membrane: how to combine fluidity and order. *EMBO J.* **25,** 3446–3457 (2006).
15. Raftopoulou, M. & Hall, A. Cell migration: Rho GTPases lead the way. *Dev. Biol.* **265,** 23–32 (2004).
16. Zaidel-Bar, R., Ballestrem, C., Kam, Z. & Geiger, B. Early molecular events in the assembly of matrix adhesions at the leading edge of migrating cells. *J. Cell Sci.* **116,** 4605–4613 (2003).
17. Del Pozo, M. A. *et al.* Integrins regulate GTP-Rac localized effector interactions through dissociation of Rho-GDI. *Nature Cell Biol.* **4,** 232–239 (2002).
18. Nayal, A. *et al.* Paxillin phosphorylation at ser273 localizes a GIT1-PIX-PAK complex and regulates adhesion and protrusion dynamics. *J. Cell Biol.* **173,** 587–599 (2006).
19. ten Klooster, J. P., Jaffer, Z. M., Chernoff, J. & Hordijk, P. L. Targeting and activation of Rac1 are mediated by the exchange factor β-Pix. *J. Cell Biol.* **172,** 759–769 (2006).
20. Ji, L., Lim, J. & Danuser, G. Fluctuations of intracellular forces during cell protrusion. *Nature Cell Biol.* **10,** 1393–1400 (2008).
21. Choi, C. K. *et al.* Actin and alpha-actinin orchestrate the assembly and maturation of nascent adhesions in a myosin II motor-independent manner. *Nature Cell Biol* **10,** 1039–1050.
22. Narumiya, S., Ishizaki, T. & Watanabe, N. Rho effectors and reorganization of actin cytoskeleton. *FEBS Lett.* **410,** 68–72 (1997).
23. Yamana, N. *et al.* The Rho-mDia1 pathway regulates cell polarity and focal adhesion turnover in migrating cells through mobilizing Apc and c-Src. *Mol. Cell. Biol.* **26,** 6844–6858 (2006).
24. Palazzo, A., Cook, T., Alberts, A. & Gundersen, G. mDia mediates Rho-regulated formation and orientation of stable microtubules. *Nature Cell Biol.* **3,** 723–729 (2001).
25. Rodriguez, O. C. *et al.* Conserved microtubule-actin interactions in cell movement and morphogenesis. *Nature Cell Biol.* **5,** 599–609 (2003).
26. Del Pozo, M. A., Price, L. S., Alderson, N. B., Ren, X. D. & Schwartz, M. A. Adhesion to the extracellular matrix regulates the coupling of the small GTPase Rac to its effector PAK. *EMBO J.* **19,** 2008–2014 (2000).
27. Hodgson, L., Nalbant, P., Shen, F. & Hahn, K. Imaging and photobleach correction of Mero-CBD, sensor of endogenous Cdc42 activation. *Methods Enzymol.* **406,** 140–156 (2006).
28. Hodgson, L., Shen, F. & Hahn, K. Biosensors for characterizing the dynamics of Rho family GTPases in living cells. *Curr. Protoc. Cell Biol.* (in the press).

Supplementary Information is linked to the online version of the paper at www.nature.com/nature.

Acknowledgements We acknowledge funding from the Swiss National Science Foundation and the Novartis Foundation, formerly the Ciba-Geigy Jubilee Foundation (M.M.), NIH T32 GM008719 and NIH F30 HL094020 (C.W.), NIH R01 GM57464 (K.M.H.), NIH R01 GM71868 (G.D.), and the Cell Migration Consortium, grant U54 GM064346 from NIGMS (G.D. and K.M.H.).

Author Contributions M.M. initiated the project, conceptualized the idea of computational multiplexing, wrote all image analysis software pertinent to multiplexing, and contributed to the writing of the manuscript; L.H. developed simultaneous imaging of RhoA and Cdc42, including the modification and validation of the meroCBD probe, developed the intermolecular RhoA sensor, including controls and validation, studying the effects of biosensor stoichiometry and expression level, developed the new version of the Rac biosensor, and contributed to writing of the manuscript; C.W. produced stable cell lines of the intermolecular RhoA biosensor and conducted imaging experiments for the comparison of intra- and intermolecular biosensor designs; H.E. contributed simulations for validation of the correlation analysis and assisted with image processing; O.P. and P.N. contributed image data of RhoA and Cdc42 activity, respectively; A.A. and G.L.J. contributed valuable advice and unpublished reagents; K.M.H. and G.D. coordinated the study and wrote the final version of the manuscript and supplement.

Author Information Reprints and permissions information is available at www.nature.com/reprints. Correspondence and requests for materials should be addressed to K.M.H. (khahn@med.unc.edu) or G.D. (gdanuser@scripps.edu).